Hindawi
Geofluids
Volume 2023, Article ID 6101374, 18 pages
https://doi.org/10.1155/2023/6101374

Research Article

Research on the Pore Evolution of Oil Shale under Different Thermal Treatment Temperatures Using NMR and FE-SEM Methods

Yan Xi,[1] **Jun Li**,[2,3] **Wei Lian**,[3] **Haifeng Fu**,[4] **Yue Qi**,[5] **and Yudong Tian**[5]

[1]*Beijing University of Technology, Beijing 100124, China*
[2]*China University of Petroleum-Beijing, Beijing 102249, China*
[3]*China University of Petroleum-Beijing at Karamay, Karamay 834000, China*
[4]*PetroChina Research Institute of Petroleum Exploration & Development, Langfang 065007, China*
[5]*CNPC Daqing Drilling Engineering Corporation, Daqing 163311, China*

Correspondence should be addressed to Wei Lian; lianweidyx@163.com

Received 25 October 2022; Revised 4 December 2022; Accepted 18 March 2023; Published 15 May 2023

Academic Editor: Peng Tan

Underground in situ pyrolysis for oil shale extraction is currently significant; the evolutions in microstructure, porosity, and permeability parameters are essential factors in evaluating the productivity of oil shale after pyrolysis. With the underground oil shale reservoir core, obtained from Jimsar Sag in the Junggar Basin in China, as the research object, the samples were subjected to the treatment at different high temperatures (400°C, 500°C, 600°C, and 700°C). The NMR and FE-SEM experiments on oil shale samples were conducted; the T_2 relaxation spectra, pore size distribution, and porosity and permeability variation were analyzed; and the relationships between movable fluid saturation and porosity and permeability were established, respectively. The results showed that when the thermal treatment temperature increased, the porosity and permeability of oil shale rose continuously but showed different laws. With the temperature being lower than 400°C, the porosity increased slowly, and the growth rate of porosity increased rapidly when the thermal treatment temperature was higher than 500°C. In the pyrolysis temperature range of 25°C~400°C, the growth rate of permeability was relatively slow. With the continuously enhancing temperature (500°C~600°C), the growth rate of permeability accelerated rapidly. When the temperature continued to rise (700°C), the increase of permeability began to slow down. There is a nonlinear correlation between porosity and movable fluid saturation and an approximately linear correlation between permeability and movable fluid saturation. The findings showed that 600°C was the suitable temperature for the pyrolysis of oil shale.

1. Introduction

Shale oil is the oil resource in organic-rich shale, a fine-grained, multipore, and microcracked sedimentary rock containing a certain amount of solid combustible organic matter named kerogen inside [1–5]. It generates several fluid components containing heavy and light oil when heated to a high temperature above 400°C [6]. On this basis, the mined oil shale is usually heated by an external heat source to reach the pyrolysis temperature to generate shale oil, including the techniques of overground retorting and underground in situ pyrolysis [7–9]. However, the overground retorting is only suitable for shallow oil shale formation and would lead to wastewater and waste gas pollution. For the reason that the depth of discovered oil shale deposits increases, underground in situ pyrolysis is more feasible for the exploitation of oil shale in the deep reservoir. In particular, this method also has the advantages of good product quality, high oil recovery rate, small footprint, and environmental protection. Laboratory tests and numerical simulation are carried out to evaluate the feasibility of in situ pyrolysis mining, such as in situ conversion process (ICP) technology from Shell, Electrofrac technology from ExxonMobil, and Crush technology from

Chevron [10–13]. The evaluation results show that this technology is conducive to the exploitation of shale oil mining. However, some problems still need to be further solved, such as the optimal heating temperature for in situ mining and how to reduce energy consumption during in situ mining. As a result, the research on underground in situ pyrolysis for oil shale extraction is of great importance.

When the underground in situ pyrolysis technique is adopted for extracting shale oil, two critical steps should be considered in the whole process. The first is the product of heated oil shale at different thermal treatment temperatures. Comprehensive research on organic matter decomposition has been made during the pyrolysis progress of oil shale based on numerous laboratory experiments [14–16]. It proved that the products discharged from oil shale were mainly pyrolysis oil when the temperature was at 300~475°C, and the hydrocarbon gas produced during pyrolysis was primarily methane; the content percentage of which exceeded 90% when the temperature was higher than 450°C, indicating that kerogen gradually matured under thermal treatment. The hydrocarbons progressively produced tend to become hydrocarbons with smaller molecular weights. The second is the evolution of shale microstructure during thermal treatment at different temperatures, which is mainly because the increase of porosity and generation of microcracks provides a migration path for oil and gas from the formation into the wellbore [17–20]. Kang et al. [17] studied the internal crack characteristics of oil shale at different temperatures through CT scanning experiments and pointed out that the cracks generated during pyrolysis were the decisive factor that can control the change in oil shale permeability. Therefore, Tiwari et al. [19] adopted CT scanning technology to investigate the changes in the pore structure of oil shale based on the high temperature of 350~500°C. Moreover, it was proposed that the high temperature caused many pores inside the rock, and the permeability increased significantly. In addition, Saif et al. [18] explored the evolution law of the generation, expansion, connectivity, and closure of pores and cracks in oil shale pyrolysis through CT scanning technology. According to the results, the first microcrack appeared at 354°C. As the temperature increased, the fractures continued to develop. Furthermore, the evolution of microcracks was dependent not only on organic matter but also on the progress of adjacent fractures. Similar findings were also made in the study by other scholars. According to the research mentioned above, it can be observed that high temperature treatment enhances the size and number of pores and microcracks in oil shale, which in turn leads to a significant increase in permeability. However, many studies ignore the influence of movable fluid on oil and gas migration in this process.

Based on previous studies, it can be known that the fluid in the reservoir rock mass can be categorized into movable and irreducible fluid according to the state of residence [21–23]. Among them, movable fluid refers to the fluid in the large pores that is weakly affected by the rock skeleton and can flow freely under a specific driving force. The irreducible fluid refers to the fluid that is tightly adsorbed in the tiny pores or the wall of large pores under the capillary pressure and surface tension. The irreducible fluid reduces the pore's flow space and obstructs the percolation channel. Many studies have been carried out on unconventional oil and gas reservoir matrix movable fluid and irreducible fluid under room temperature [23–26]. It can be seen that the changes in porosity and permeability can, to a certain extent, but cannot fully characterize oil and gas productivity. It is necessary to consider the proportion of movable fluid in the total saturated fluid, which can characterize reservoir properties. As a result, it is not sufficient to scientifically evaluate the oil and gas production efficiency for the oil shale heated in situ, based on the analysis of the change law of porosity and permeability under different thermal treatment temperatures. Based on the above analysis, it can be seen that it is necessary to explore and analyze the microstructure changes of oil shale under different thermal temperatures during in situ heating and quantify the porosity and permeability characteristics and movable fluid saturation on this basis to serve as a reference for evaluating shale oil production efficiency.

Nuclear magnetic resonance (NMR) technology, a recognized nondestructive technique, has been used to measure porosity and pore distribution in shale, which can be used for calculating the saturation of movable fluid [27, 28]. In the process of analyzing the movable saturation in the oil shale reservoir matrix, the critical data T_2 relaxation spectra can be used to distinguish between adsorption pores and infiltration pores, which are important parameters that affect the calculation of movable fluid saturation. The boundary between the two is known as the T_2 cut-off value, and it can be calculated based on the centrifugal calibration method. A pore with transverse relaxation time that is less than the T_2 cut-off value is named adsorption pore. Besides, a pore with a transverse relaxation time higher than the T_2 cut-off value is called infiltration pore. The fluid in the adsorption pore that cannot flow freely under the action of the capillary force is called irreducible fluid, while the fluid in the infiltration pore that can deal with the capillary pressure and flow freely is called movable fluid. Most existing studies on conventional reservoir matrices do not consider the effect of different thermal treatment temperatures. For the oil shale matrix, its microstructure changes continuously with the increase of thermal treatment temperature, which will lead to the change in the number and sizes of pores and microcracks; then, the T_2 cut-off value changes accordingly. Therefore, the analysis of shale oil production at different thermal treatment temperatures requires calculating the T_2 cut-off value, to be used to accurately analyze the movable fluid saturation of oil shale after the change of microstructure.

With the underground oil shale reservoir core as the research object, the samples were treated at high temperatures (400°C, 500°C, 600°C, and 700°C). In addition, the microscopic changes of oil shale at various temperatures were explored by adopting field emission-scanning electron

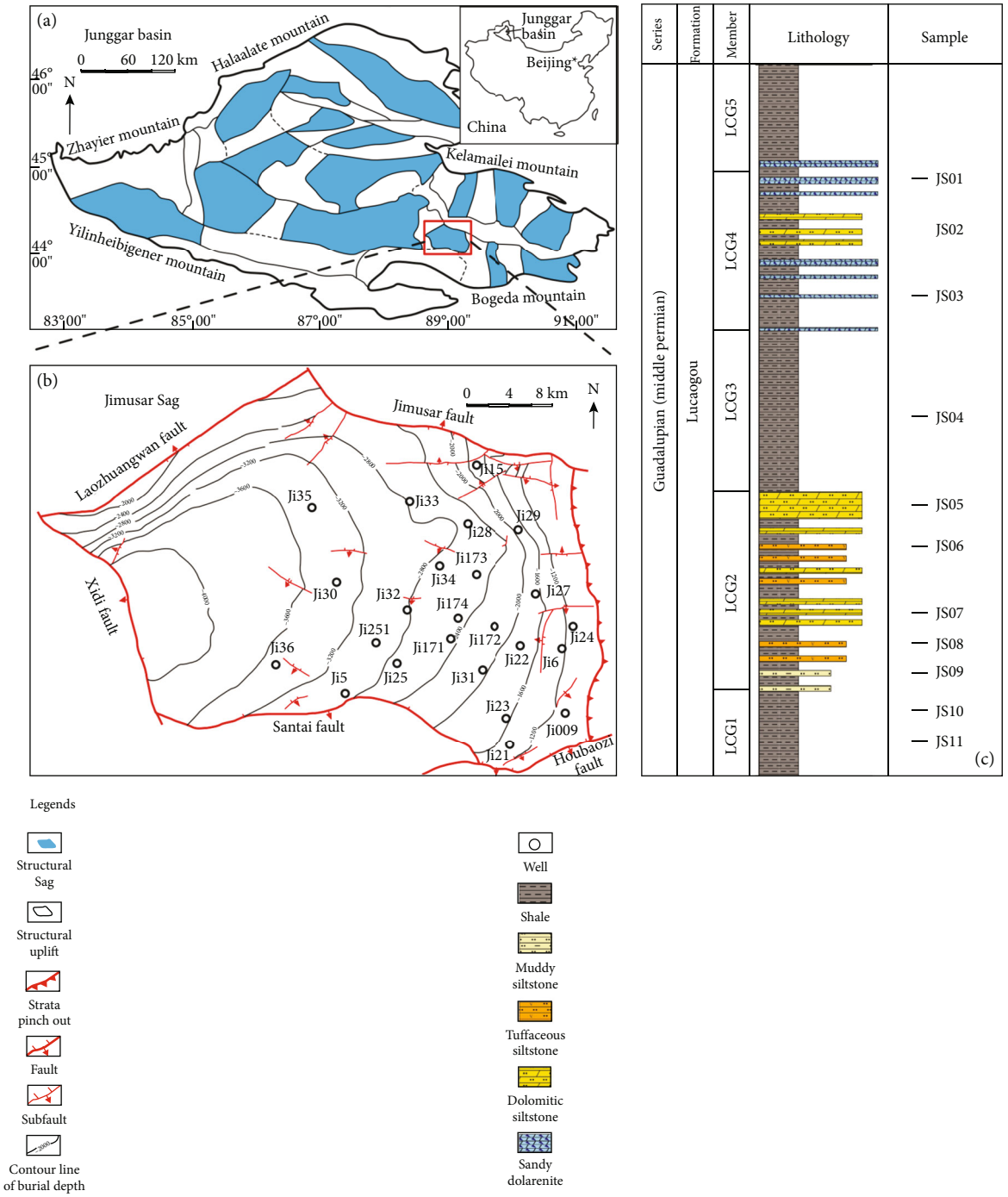

Figure 1: Detailed geological information of Junggar Basin's Jimsar Sag [29].

microscopy (FE-SEM) experiments, and the generation and development of pores and microcracks were analyzed. Meanwhile, low-field NMR scanning technology was adopted for analyzing the T_2 relaxation spectra, pore size distribution, porosity, and permeability variation of the samples before and after pyrolysis, the variation of T_2 cut-off value and movable fluid saturation at different temperatures, and the relationship between porosity and permeability and their relationship with movable fluid saturation. The results can provide a reference for optimizing in situ pyrolysis parameters and productivity prediction of oil shale.

2. Materials and Experimental Methods

2.1. Sample Description. The Jimsar Sag, with its position in the southwestern part of the East Junggar Basin, is a small oil-abundant depression of about 1.2×10^3 km^2 in area (Figure 1(a)). With its shape resembling a dustpan, the sag was deposited on a Carboniferous fold basement, which has experienced multiphase tectonic movements. The depression has definite boundaries, whose inner structure and topography are mild (Figure 1(b)). Due to the local tectonic expansion, fast sag subsidence occurred in the early Mid-Permian

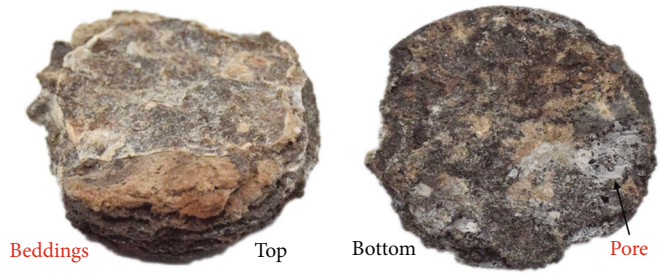

Figure 2: Oil shale samples from the reservoir.

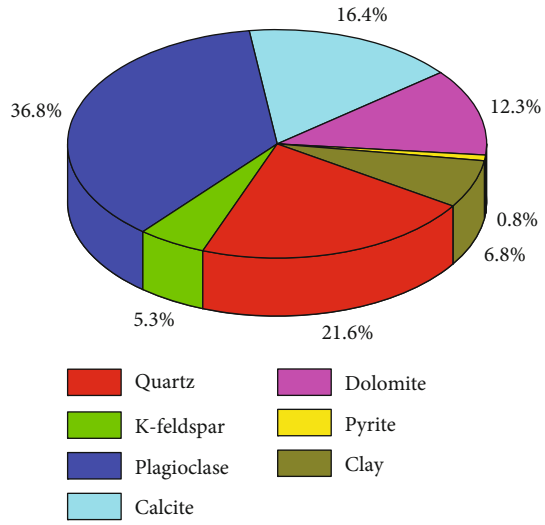

Figure 3: Mineralogical composition measured by X-ray diffraction.

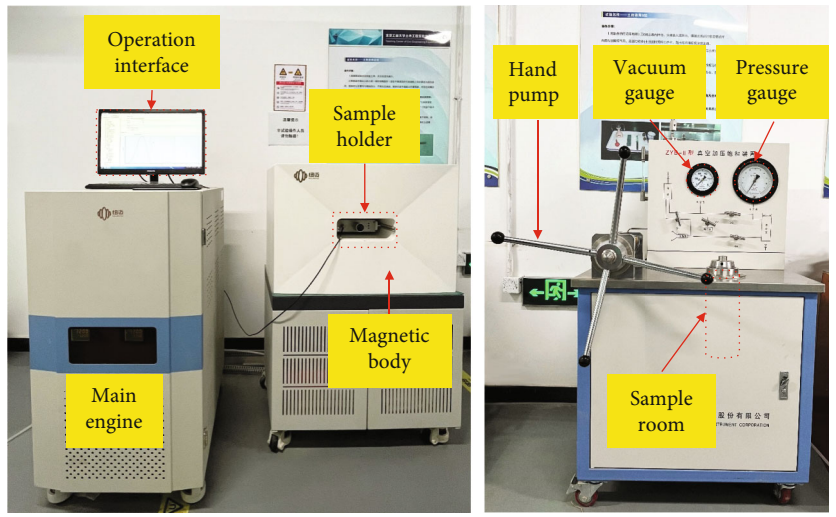

NMR instrument Vacuum saturation instrument

Figure 4: Vacuum saturation and NMR instrument.

period, and entire sag deposition occurred in the Mid-Permian–Cenozoic period. The Mid-Permian Lucaogou Formation, which is 100~300 m thick, was deposited under a saline lacustrine context. It comprises a complicated sequence of shale, dolomitic/muddy/tuffaceous siltstone, and sandy dolerite, which are the predominant reservoir rocks with varying oiliness.

Jimsar shale oil underground Lucaogou formation core was used as the research object, which can be found in Figure 2. The core has apparent wavy bedding, as well as

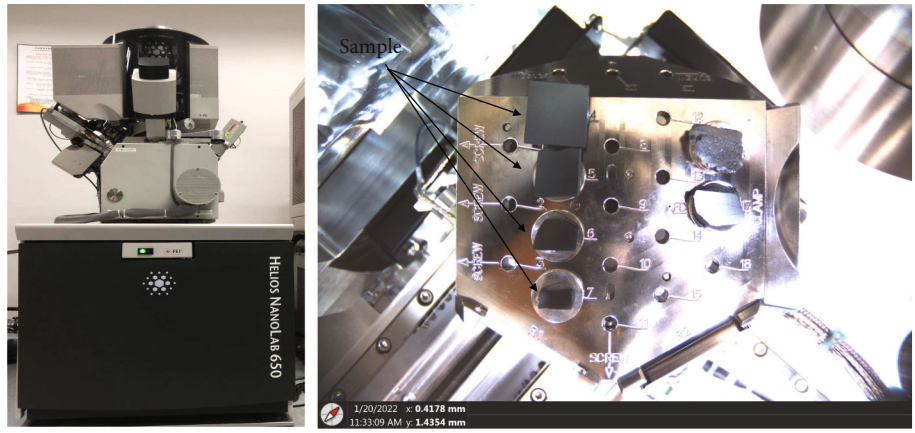

Figure 5: FE-SEM equipment and core sampling.

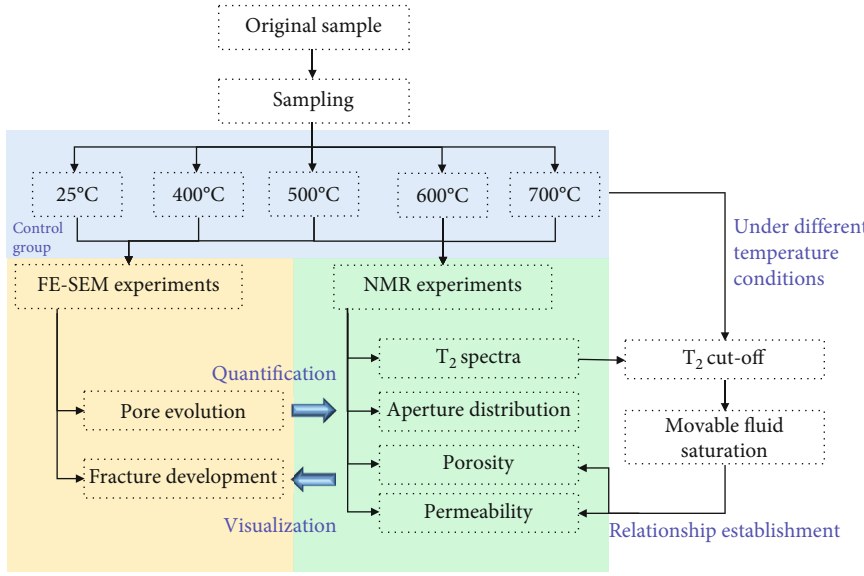

Figure 6: Experimental procedure.

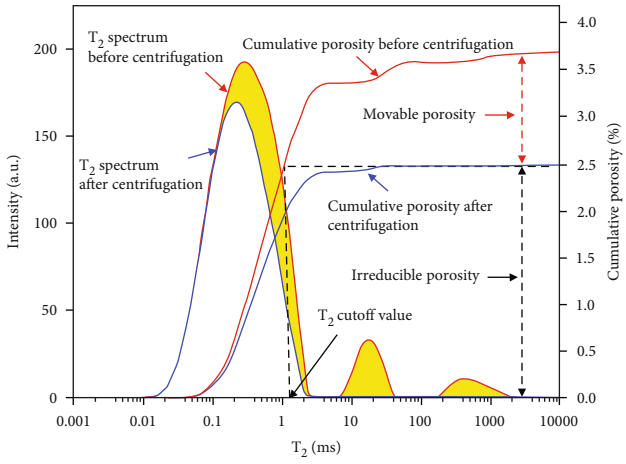

Figure 7: Cut-off value calculation method.

noticeable pores on the surface. With the purpose of profoundly clarifying the composition of the rock sample, the rock sample was subjected to X-ray diffraction analysis before testing. According to the analysis results, the rock samples are mainly composed of quartz (21.6%), plagioclase (36.8%), calcite (16.4%), and dolomite (12.3%), as well as a small number of clay minerals (6.8%) and pyrite (0.8%), as shown in Figure 3.

2.2. Experimental Equipment and Procedures

2.2.1. NMR Experiments. Nuclear magnetic resonance (NMR) technology can be used as characteristic parameters of porosity and permeability in the rock mass [30]. In this paper, the device of Micro MR12-025V LF NMR was used to carry out the experiments, as shown in Figure 4. During measurement, the laboratory temperature was constant at $25.00 \pm 0.50 \circ C$, and the magnetic field temperature was controlled at $32.00 \pm 0.02 \circ C$. The frequency of the NMR instrument was set to 12 MHz, and the test sequence

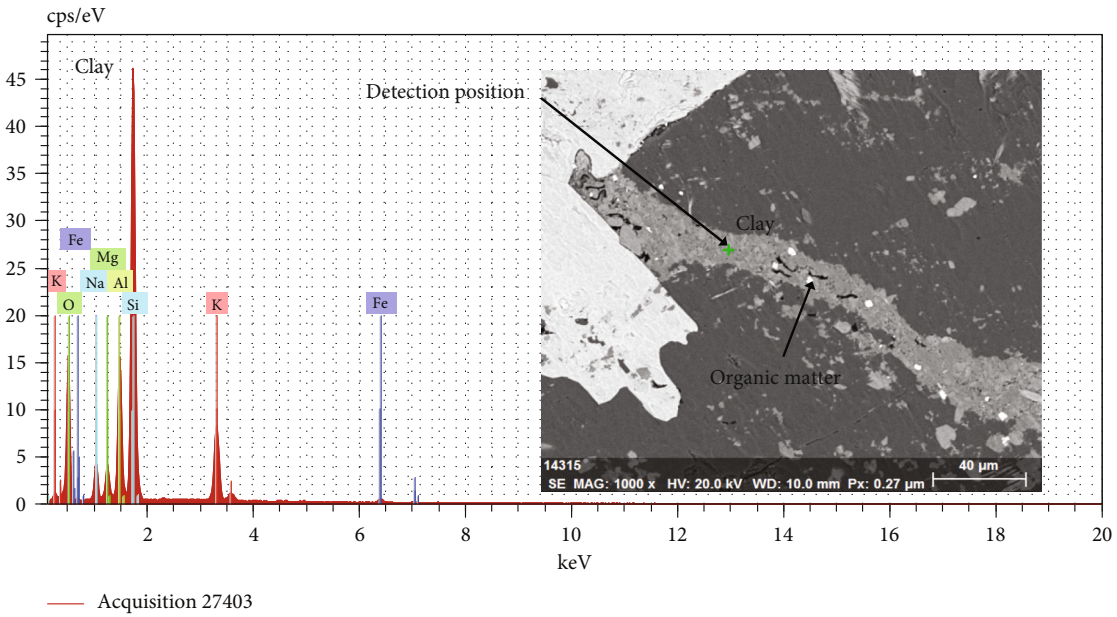

Figure 8: FE-SEM measurement results at room temperature.

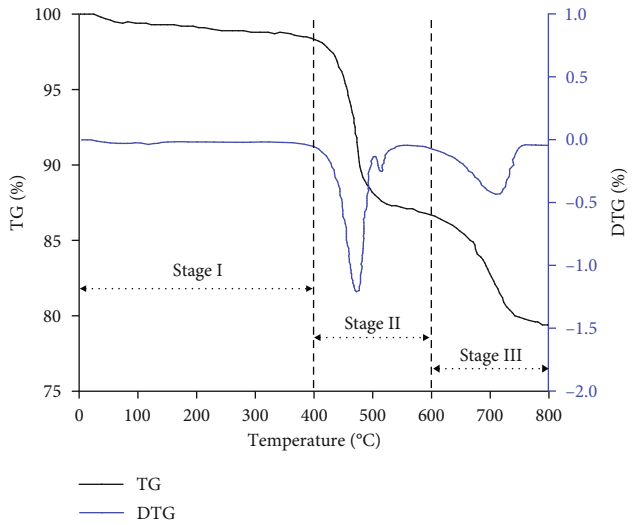

Figure 9: Thermogravimetric test curves.

adopted the CPMG sequence. Other main parameters were set as follows: echo interval (TE) = 0.1 ms, sampling interval (TW) = 3000 ms, number of echoes (NECH) = 8000, and cumulative sampling number (NS) = 128.

2.2.2. FE-SEM Experiments. In order to observe the evolutions in pores and microcracks of oil shale core before and after thermal treatment, argon-ion polishing field emission-scanning electron microscopy (FE-SEM) was employed to feature the microscopic pore structure properties of shale samples [31], as shown in Figure 5. In argon ion polishing, a suitable small piece was first removed from a larger sample, which was mechanically cut and ground into smooth flakes and then polished with an argon ion polisher. Under the electric field, the argon gas was ionized into positively charged argon ions based on certain energy. Argon ions flew from the anode to the cathode and passed through the cathode hole to the sample surface. Under the constant bombardment of argon ions, the surface of the sample becomes smooth and flat. After argon ion polishing, the dense oil shale has extremely high flatness. The high-quality flat surface cleared the boundaries between mineral grains, thus increasing the identification of different mineral grain size ranges. This method enabled efficient identification and observation of organic matter and its internal nanopores for oil shale, revealing the chemical composition within the microregion.

2.2.3. Experimental Procedures. During the test, the test samples were divided into two groups. The specific experimental process is as follows (Figure 6).

Group 1 experimental samples were used in the FE-SEM experiments, and a total of four pieces were included. Each

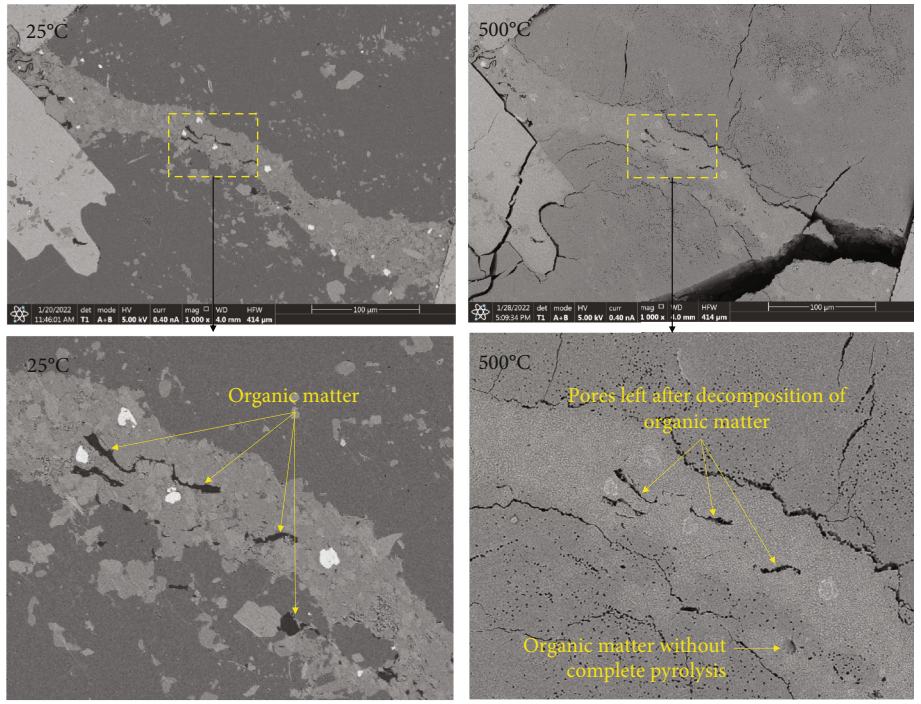

Figure 10: FE-SEM measurement results before after thermal treatment.

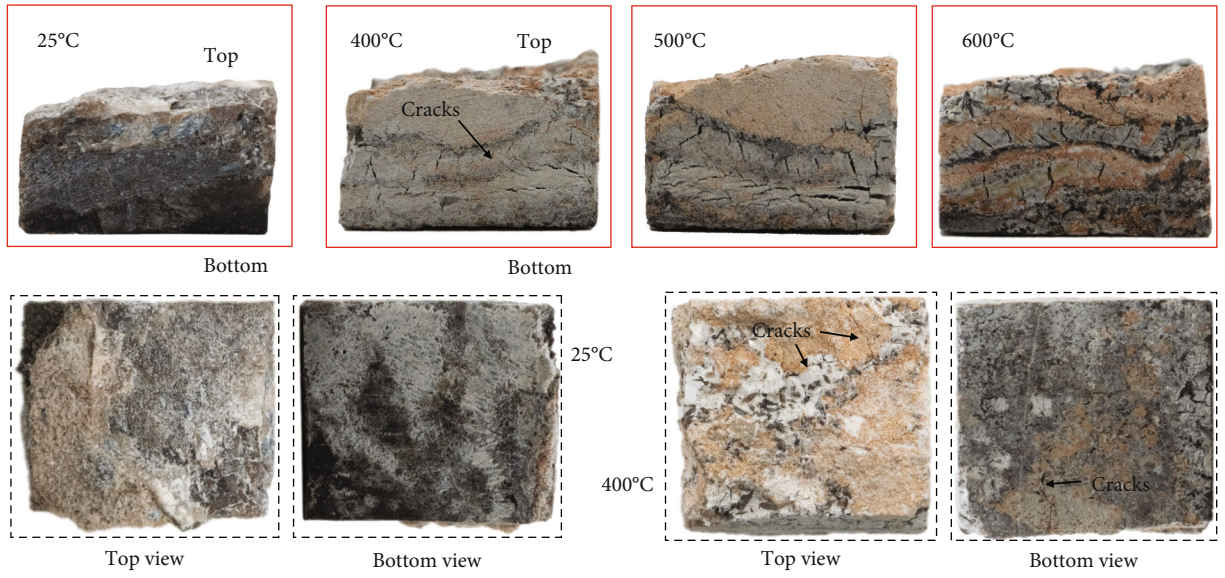

Figure 11: Sample morphology after high-temperature treatment.

rock sample was first observed at room temperature. Then, the samples were treated at the temperature of 400°C, 500°C, 600°C, and 700°C for three hours. Finally, the changes in pores and cracks at the same positions were observed using the FE-SEM method.

Group 2 experimental samples were used for low-field NMR testing. Residual moisture in the original sample was removed before testing. The samples were evacuated for 24 hours at room temperature and then placed in a drying oven to dry to constant weight (60°C, five hours). The other samples were heated to 400°C, 500°C, 600°C, and 700°C, separately. All samples were placed in a vacuum pressurized saturation device for 12 hours to reach a 100% saturated water state. The wet weight of samples was used for the calculation of sample volume. A low-field NMR analyzer subjected the saturated water samples to saturated water NMR experiments. The saturated water state obtained the T_2 relaxation spectra through the inversion calculation. After completing the NMR test of the saturated water samples, the samples were subjected to high-speed centrifugation at 6500 (rpm) (centrifugal pressure of 1.42 MPa) to discharge movable water in accordance with the oil and gas industry

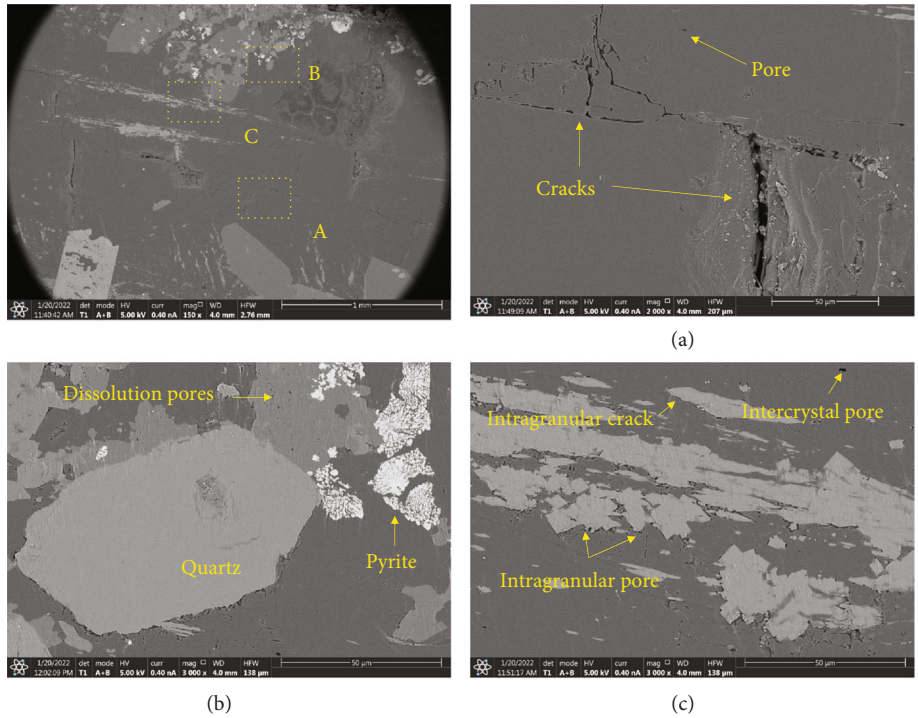

Figure 12: FE-SEM measurement results at room temperature.

standard SY/T5336-2006. In addition, the centrifuged samples were retested by NMR to obtain the T_2 relaxation spectra in an irreducible water state.

2.3. Calculation Method of Movable Fluid Saturation. Movable fluid is mainly found in the middle of larger pores, and the force of rock skeleton is relatively tiny, so it has better fluidity under a specific external driving force. The analysis of movable fluid saturation at different temperatures is significant to studying pyrolysis temperature's influence on oil and gas production efficiency. The movable fluid saturation can be measured in accordance with low field NMR measurement results.

The T_2 relaxation spectra are an essential parameter for calculating movable fluid saturation because there is a specific relationship between the T_2 relaxation spectra and the pore size distribution. Besides, the T_2 relaxation spectra can be used to quantitatively analyze the adsorption hole and seepage hole in the rock, and the boundary value between them is called T_2 cut-off value (T_{2c}), which is also the movable fluid cut-off value. After centrifugation, T_2 cut-off value can be obtained by saturated water T_2 relaxation spectra and irreducible water T_2 relaxation spectra. The specific process is as follows: Based on the T_2 relaxation spectra before and after centrifugation, draw the corresponding porosity accumulation curve, respectively, and draw a horizontal line from the maximum value of the porosity accumulation curve after centrifugation Figure 7. The T_2 value corresponding to the intersection of the horizontal line and the porosity accumulation curve before centrifugation is T_{2c}.

The pores in consistence with the transverse relaxation time less than T_{2c} ($T_2 < T_{2c}$) are called adsorption pores, while the pore in consistence with the transverse relaxation time greater than T_{2c} ($T_2 > T_{2c}$) is called seepage pore. The fluid in the adsorption pore cannot flow freely under the action of capillary force, which is named bound fluid. The fluid in the seepage hole can flow freely against the capillary force, which is called movable fluid Figure 8.

Then, the movable fluid saturation can be depicted by the ratio of movable fluid volume to the saturated fluid volume of the rock sample:

$$S_{wm} = \frac{\int_{T_{2c}}^{T_{2\,\max}} S(T_2)dT_2}{\int_{T_{2\,\min}}^{T_{2\,\max}} S(T_2)dT_2 t} \times 100\%, \quad (1)$$
$$S_{wi} = 1 - S_{wm},$$

where $T_{2\min}$ and $T_{2\max}$ represent the maximum and minimum of the T_2 relaxation spectra, respectively, ms; T_{2c} is the T_2 cut-off value, ms; and $S(T_2)$ is the expression of the T_2 relaxation spectra distribution curve.

3. Experimental Results

3.1. Thermogravimetric Analysis

3.1.1. Analysis of Pyrolysis Curve. Meanwhile, an STA/HP150 thermal synchronous analyzer was adopted to measure derivative thermogravimetric (DTG) and thermogravimetric (TG). The sample size was controlled at 9.0 ± 0.1 mg during the test. The starting temperature of the TG-DTG curve reached 25°C, the heating rate was ten °C/min, and the final reaction temperature was 800°C.

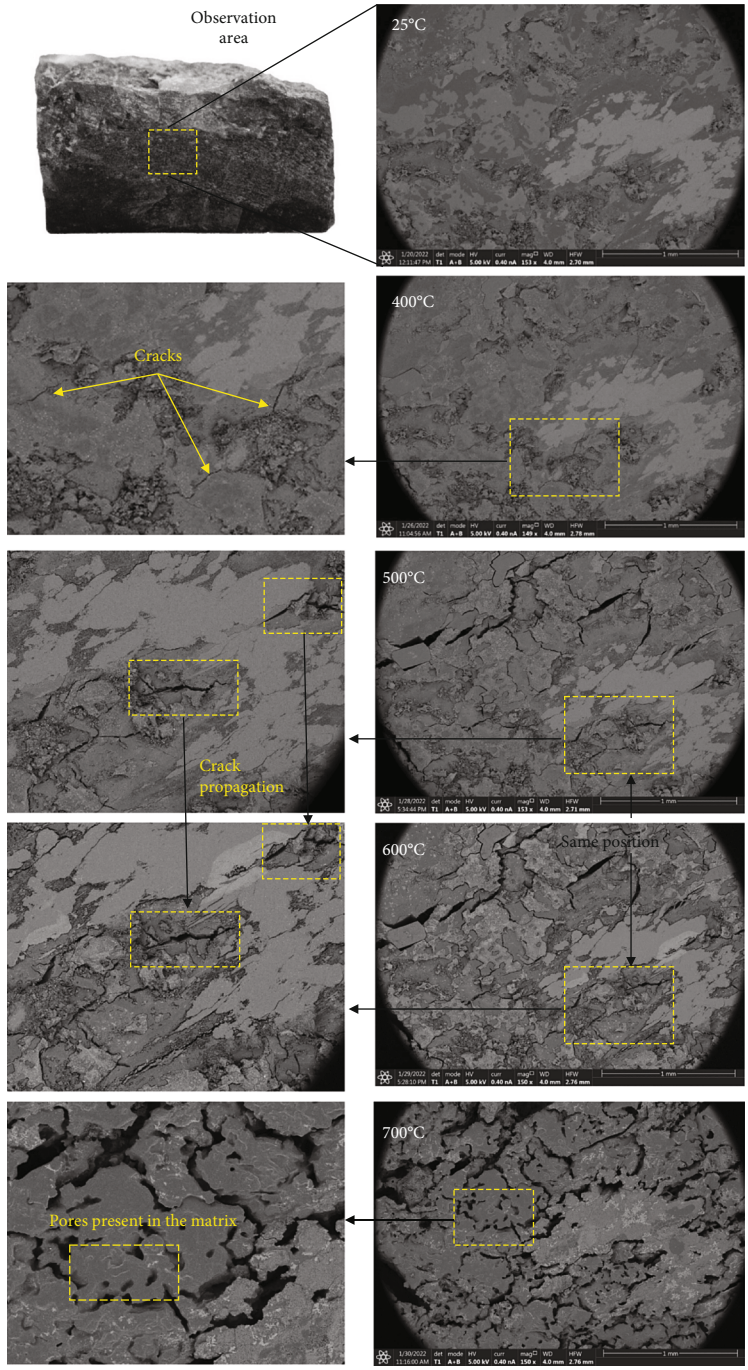

Figure 13: FE-SEM measurement results during thermal treatment.

Figure 9 shows the TG and DTG results of the oil shale samples under a high-purity N_2 atmosphere. The stages were as follows:

Stage I: during the continuous heating of rock samples from room temperature (25°C) to 400°C, the weight loss of oil shale is about 1.7% of the total mass of the sample, as well as 8.6% of the total weight loss. The TG curve decreases slowly in this temperature range, and the DTG curve fluctuates less. The mass loss mostly contained water evaporation, like adsorption water evaporation in clay minerals and interlayer water evaporation. At the same time, some organic matter appeared during preliminary pyrolysis.

Stage II: with the continuous increase of thermal temperature (400°C~600°C), significant mass loss was found in the temperature range. The weight loss of oil shale is about 11.3% of the total mass of the sample and 56.8% of the total weight loss of oil shale. The TG curve drops sharply in this temperature range, and the DTG curve fluctuates significantly.

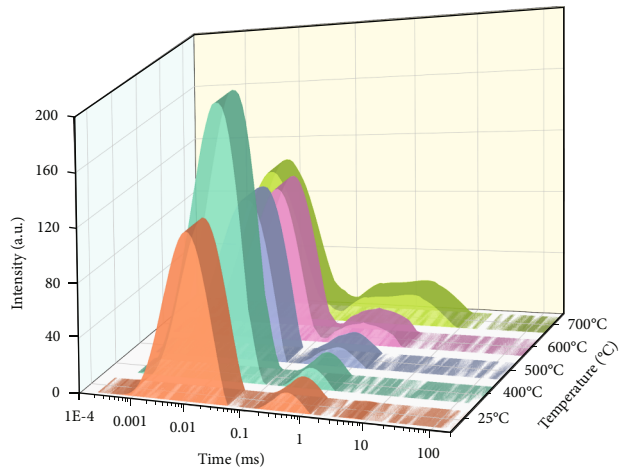

Figure 14: NMR T_2 spectra at different temperatures.

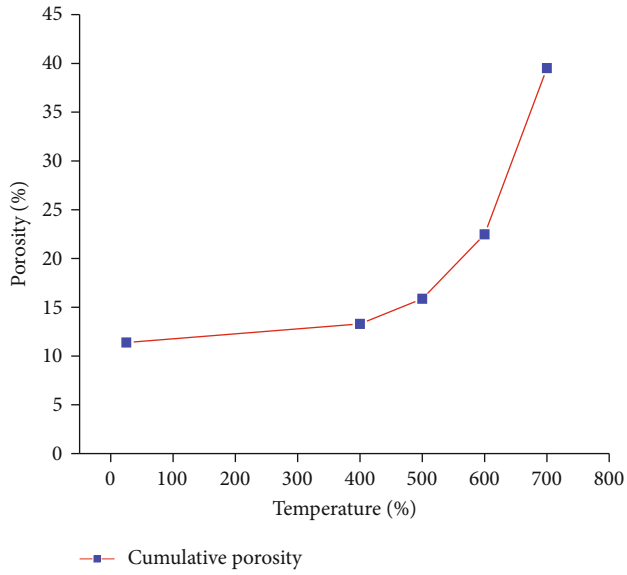

Figure 15: Variation of porosity at different temperatures.

The weight loss of oil shale is mainly the weight loss of organic matter pyrolysis, which is primarily manifested by the thermal cracking reaction of kerogen.

In the initial pyrolysis stage, many unstable bridge bonds undergo bond-breaking reactions, and then, the broken chemical bonds are further recombined to form light gases. With the increase in temperature, a large amount of organic matter in the oil shale is pyrolyzed, and asphaltene is generated. With the continuous pyrolysis of asphaltene, a large amount of oil, gas, and oil shale semicoke is generated. With the overflow of oil and gas, the weightlessness of the oil shale gradually increases.

Stage III: when the temperature is more than 600°C, the weight loss of oil shale (7.2%) is mainly caused by the secondary cracking reaction of products and the decomposition of minerals such as carbonate.

3.1.2. Loss of Organic Matter during Pyrolysis. To explore the pyrolysis process of oil shale in detail, the decomposition of organic matter at room temperature and during the heating process was observed by FE-SEM. Figure 8 shows the FE-SEM measurement results at room temperature. It can be seen that clay minerals exist in the rock sample, and obvious organic matter can be observed, filling the corresponding pore positions at room temperature.

Figure 10 shows the comparison results of oil shale samples at room temperature and after thermal treatment (500°C). According to former research, it can be found that the organic matter in the rock is pyrolyzed into gas and will escape along the cracks in the rock at 500°C [6]. Three cases can be seen in Figure 10.

First, the organic matter is completely pyrolyzed at high temperatures, leaving only pores in the original position.

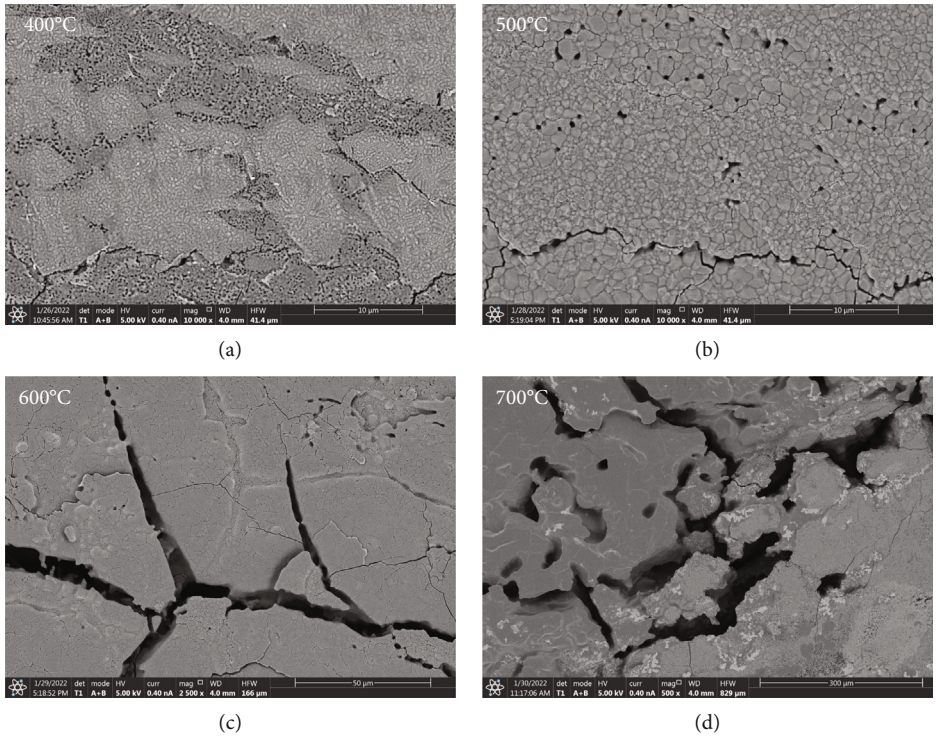

Figure 16: Evolution of pores and microcracks at different temperatures.

These pores will contribute to the increase of pores in the sample and gradually penetrate during heat treatment in order to form the path of oil and gas migration.

The second is the partial pyrolysis of organic matter, which contributes little to the increase of pores. With the rise of subsequent temperature, it will be gradually pyrolysis, which is conducive to improving the porosity of rock samples and contributing to the improvement of permeability.

Third, some pore positions containing less organic matter will also disappear after organic matter pyrolysis, mainly because the pore volume is small and the thermal expansion of rock occupies the corresponding position.

3.2. Analysis of Macroscopic and Microscopic Fracture Morphology

3.2.1. Change of Macroscopic Morphology. Figure 11 shows the changes in morphology characteristics of the oil shale samples before and after high temperature treatment. Obviously, the surface of the original piece was relatively dense at room temperature. After thermal treatment at 400°C, some microcracks appeared in the sample. When the temperature increased (500°C~600°C), the microcracks generated on the surface and inside the rock samples became more evident and complex.

During oil shale pyrolysis, the microcracks in the rock sample continue to expand, and multiple fractures begin to connect. After pyrolysis, the connected microcracks can provide a migration channel for the organic matter. However, in view of the different sizes and degree of connectivity of microcracks formed at different temperatures, it will also affect the mobility of fluid, which needs to be quantified by the low field NMR test method.

3.2.2. Changes in Microscopic Morphology

(1) Pore and Crack Morphology in the Original Form. To deeply explore the generation and development of oil shale pores and cracks during high-temperature pyrolysis, the microscopic morphology of oil shale at room temperature was observed, as presented in Figure 12. The oil shale matrix is dense and contains numerous pores and cracks containing intergranular mineral pores, intergranular cracks, and corrosion pores. Intergranular pores mainly include pores between mineral particles, pores between crystals, and pores at the edges of rigid particles, and these pore diameters are generally less than 0.1 μm. In contrast, intergranular pores have larger pore sizes (<1 μm), better connectivity, and more significant number, which exert a more critical role in the migration, seepage, and accumulation of reservoir fluids. The width of some microcracks is about 1 μm~10 μm, which is significant for enhancing permeability and movable fluid saturation after pyrolysis.

Due to many pores with minor porosity distributed in the shale matrix, microcracks can not only offer sufficient space for the storage of shale oil and gas after pyrolysis but also act as a channel for its seepage, which is conducive to the desorption and migration as well as seepage of shale oil. For reservoir modification, the existence of many

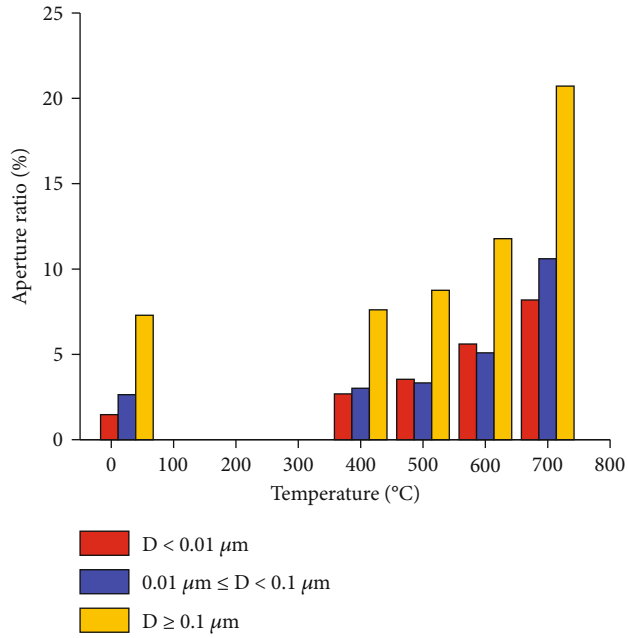

Figure 17: Changes of pores with various sizes at various temperatures.

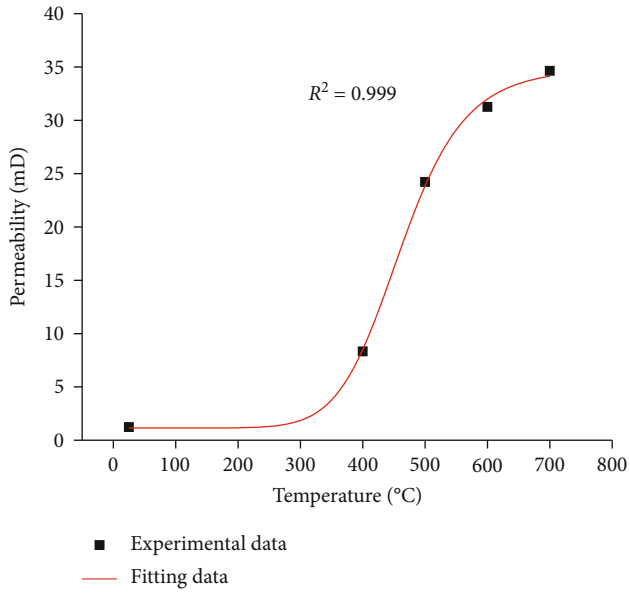

Figure 18: Variation law of permeability under different temperature.

microcracks contributes to communicating the disconnected matrix pores, thereby maximizing the formation of shale oil mining.

(2) Microcrack Evolution Morphology during Pyrolysis. To investigate the changes in pores and microcracks during the thermal treatment, the same rock sample was treated at temperatures of 400°C, 500°C, 600°C, and 700°C, as shown in Figure 13. Then, the evolutions of pores and microcracks at the same position under different heat treatment temperatures were observed.

When the image width is 2.7 mm, the oil shale is comparatively dense at room temperature (25°C), and it is challenging to see apparent pores and fractures with the naked eye. In order to further compare the evolution law of pores and fractures, the observation area and image width remain unchanged during heating.

When the heating temperature was 400°C, microcracks appeared in the oil shale matrix under thermal stress. At this point, microcracks are relatively inconspicuous and few. When the heat treatment temperature was enhanced to 500°C, the microcracks in the oil shale matrix became

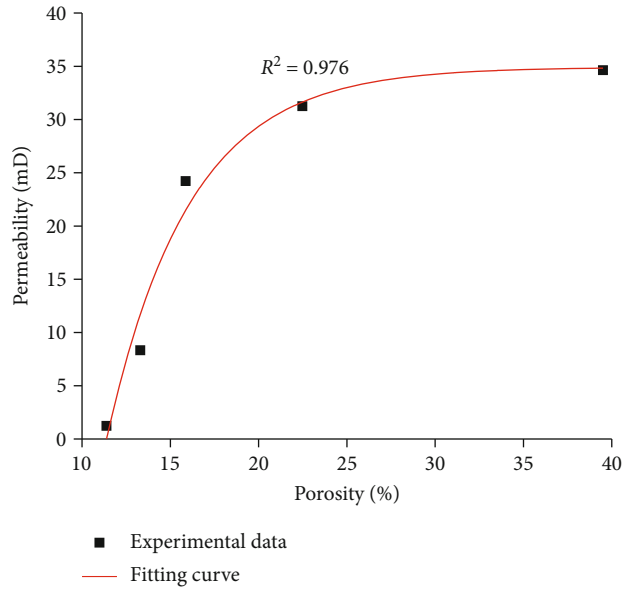

Figure 19: Relationship between porosity and permeability.

more apparent. In addition, many microcracks started to develop along the crystal edges. Because of various thermal expansion coefficients of different types of crystals, microcracks occur along the crystal edges during heating.

When the temperature continued to increase (600°C), the microcracks continued to enlarge, generating an obvious enhancement in the width and length of the microcracks. In addition, different microcracks gradually penetrated each other, and the morphology of the microcrack became more complex. With the temperature reaching 700°C, numerous pores and cracks occur in the oil shale matrix's crystals, mainly because of the pyrolysis of matrix minerals.

3.3. Analysis of Variation Law of Porosity and Permeability Characteristics

3.3.1. Analysis of T_2 Relaxation Spectra under Different Temperatures. The grain surface–pore fluid interactions are assessed by the NMR T_2 data. Theoretically speaking, larger pore bodies are indicative of longer (more significant) T_2 relaxation times, whereas smaller pore bodies have shorter (less) T_2 values. Besides, a higher signal amplitude at a particular value of T_2 in the NMR T_2 data indicates more fluid at this pore dimension. Hence, the fluid level at particular pore dimensions can be estimated by the aggregate T_2 distribution. NMR T_2 spectra at different thermal treatment temperatures (25°C, 400°C, 500°C, 600°C, and 700°C) are presented in Figure 14.

At room temperature (25°C), the T_2 spectra showed a bimodal shape. Furthermore, the double peaks were isolated from each other, which indicated numerous tiny pores and some big pores in the rock matrix with poor connectivity between different levels of pores.

As the temperature increases from 25°C to 400°C, the area on the left side increases, which means that when heated to 400°C, the small pores in the sample with thermal stress increase. There is little change in the area on the right, which means that there are few macropores at this temperature, which has no significant impact on the measurement results.

When the temperature continued to increase (500°C), the area of the left side decreased, but the area of the right area increased, mainly due to the aggregation of some tiny pores into large pores. When the temperature continuously rises (600°C~700°C), the isolated state of the two areas of saturated water T_2 relaxation spectra changes. Some fusion between the two regions indicates that in situ pyrolysis led to a marked increase in connectivity between different grades of pore size.

According to the NMR relaxation mechanism analysis, oil shale pore structure was significantly changed during the thermal treatment.

3.3.2. Variation Law of Porosity under Different Temperatures. Figure 15 shows the oil shale porosity variation law under different treatment temperatures. It can be seen that, with the increasing treatment temperature, the oil shale porosity increases. The specific rules are as follows.

The porosity increases slowly when the heat treatment temperature is lower than 400°C, and the porosity increases gradually. At the temperature of 400°C, the porosity (13.31%) is only 16.85% higher than that at room temperature (11.39%). In this stage, the temperature makes the pores and microcracks produced by the oil shale relatively small, as shown in Figure 16(b).

With the thermal treatment temperature being higher than 500°C, the increase rate of porosity is progressively accelerated. The number of pores in the oil shale matrix increases with obvious microcracks at this thermal treatment temperature, as found in Figure 16(b).

With the temperature reaching 600°C, the growth rate of porosity is more prominent. The microcracks on the oil shale matrix are more pronounced and continuously penetrated,

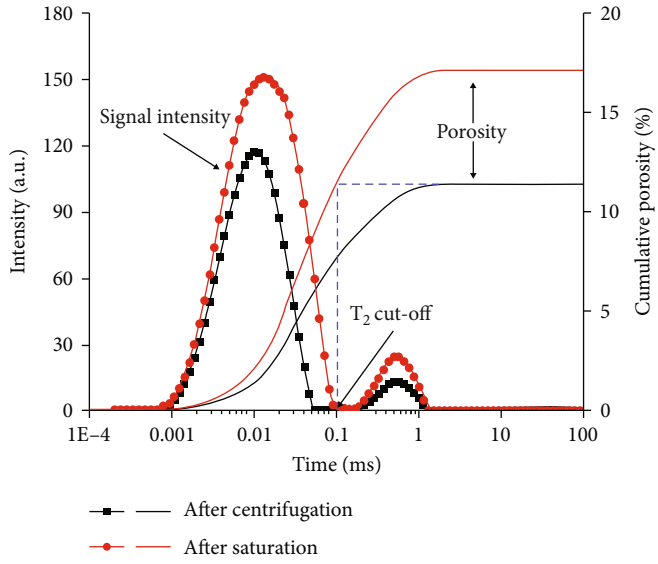

Figure 20: T_2 cut-off calculation value at room temperature.

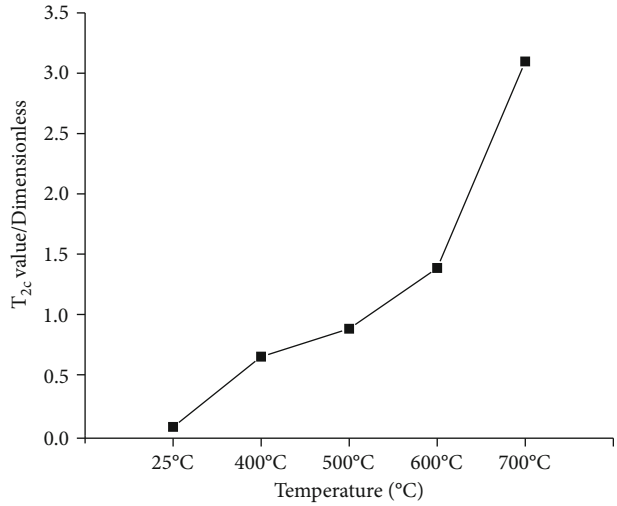

Figure 21: Variation law of T_2 cut-off value.

resulting in a significant increase in porosity, as shown in Figure 16(c).

When the temperature is 700°C, the pores and cracks on the oil shale matrix begin to penetrate, providing better transport paths for gas output, as shown in Figure 16(d).

In order to quantify the changes in pore size, the changes in pores with various sizes at various temperatures are shown in Figure 17. Based on previous studies, the large, medium, and small apertures are defined as follows: a pore with a pore size below 0.01 μm is defined as the small pore size, a pore with a pore size of 0.01~0.1 μm is defined as the medium pore, and a pore with a pore size larger than 0.1 μm is defined as the big pore.

It can be observed from Figure 17 that during the process of enhancing the temperature from 25°C to 400°C, there is an apparent enhancement in the small pores, but the increase in big pores is limited. When the temperature deeply enhances (500°C), both small and medium pores increase with insignificant magnitudes. With the temperature reaching 600°C, the apparent enhancement in the three pores exists. With the enhancing temperature of 700°C, the growth of big pores is the most significant.

3.3.3. Variation Law of Permeability under Different Temperature. The increase of pores and microcracks inevitably generates an enhancement in permeability. Figure 18 shows the variation law of oil shale permeability under different temperatures. From this figure, the permeability is found to enhance constantly with the increasing heat treatment temperature. In addition, the growth rate of permeability varies significantly in each temperature interval.

In the pyrolysis temperature range of 25°C~400°C, the number of pores is small with poor connectivity, leading to a weak increase in permeability (from 1.23 mD to 8.33 mD). From 500°C, the number of pores increases, and the pore size becomes more extensive. In particular,

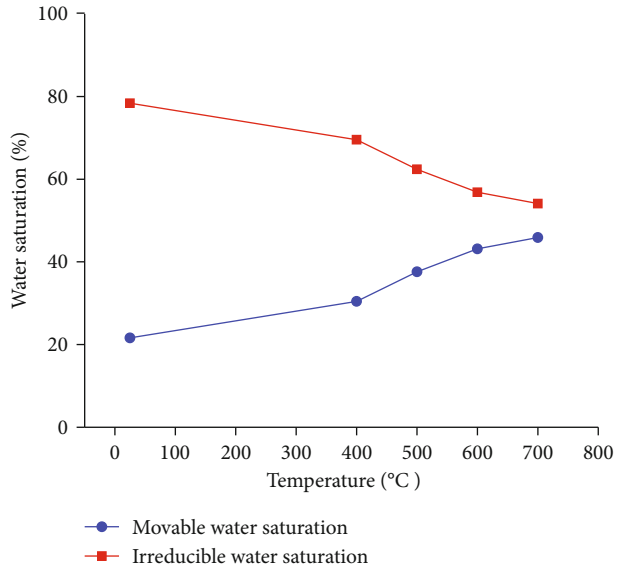

Figure 22: Variation law of movable water saturation and irreducible water saturation.

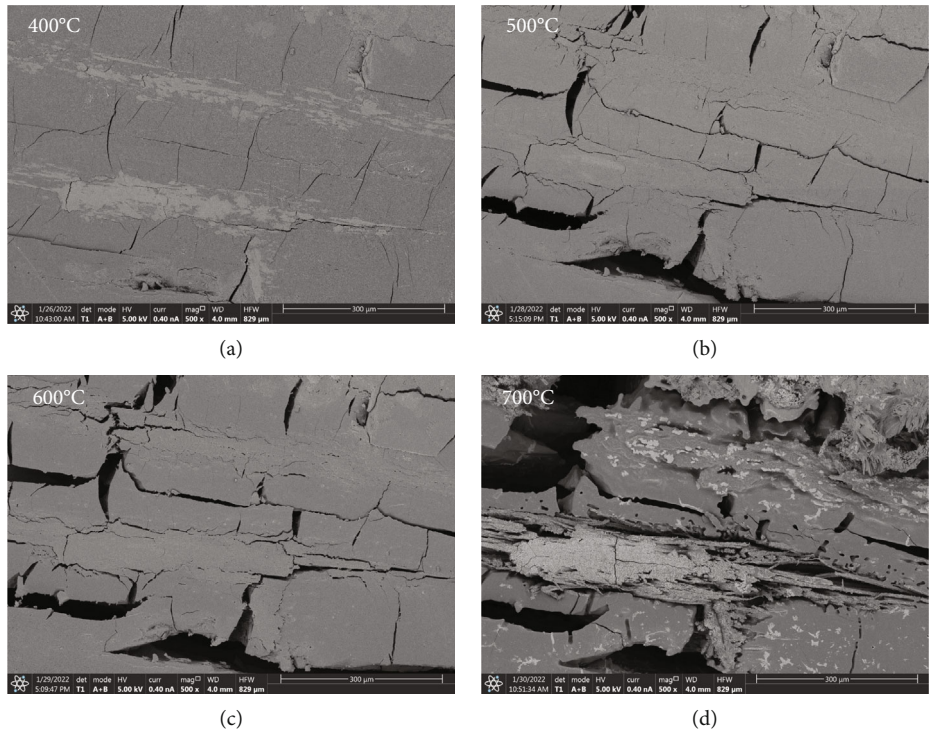

Figure 23: Generation and evolution of microcracks at different temperatures.

the increase in movable fluid porosity leads to improved pore connectivity and accelerated permeability growth (24.22 mD). With the temperature reaching 600°C, the NMR permeability is 31.25 mD, increasing with the enhancement of treatment temperature. When the temperature continues to rise (700°C, 34.63 mD), the increase of permeability begins to slow down.

Thermal treatment changes the porosity and microstructure of oil shale and then affects the permeability of oil shale. The relationship between the two parameters can be used to predict permeability based on porosity, considering the influence of pyrolysis temperature, as presented in Figure 19. Obviously, as porosity increases with the thermal treatment temperature, permeability increases.

The fit of porosity and permeability was performed to clarify the relationship between the two parameters ($R^2 = 0.976$); a nonlinear association exists between porosity and permeability. With the thermal treatment temperature

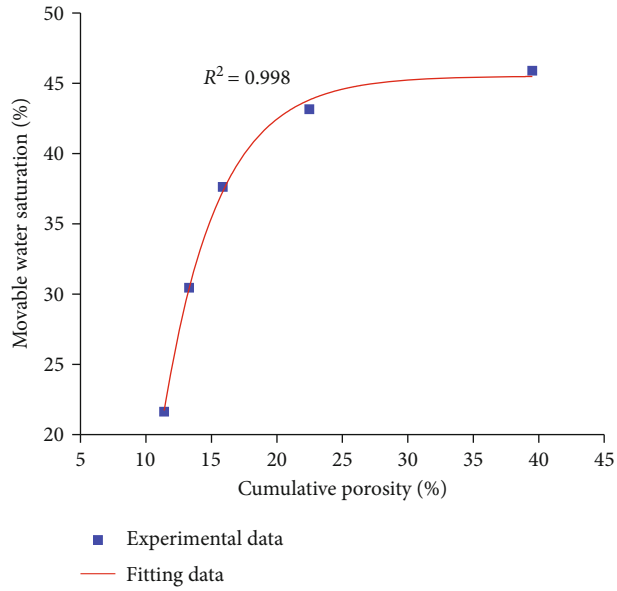

Figure 24: Correlation between movable fluid saturation and porosity.

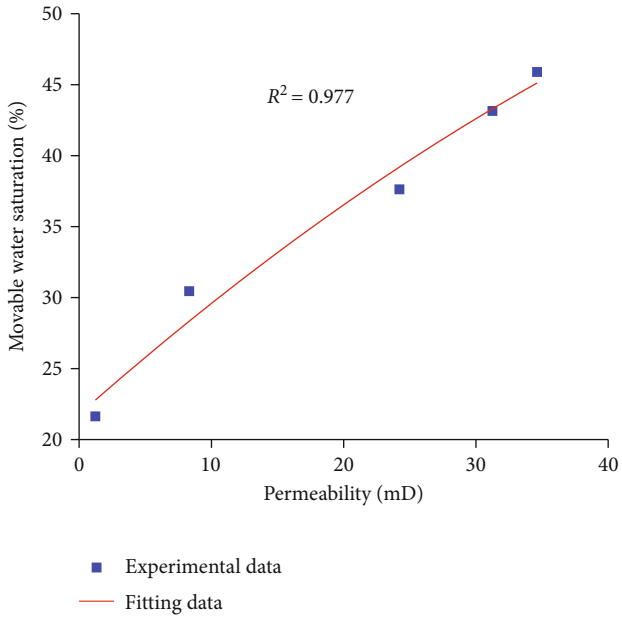

Figure 25: Relationship between permeability and fluid production capacity.

lower than 600°C, the permeability enhances quickly when porosity increases. With the continuous enhancement of thermal treatment temperature (700°C), the growth rate of permeability gradually slows down. It shows that 600°C is the suitable temperature for oil shale pyrolysis.

4. Discussion

4.1. Analysis of Movable Fluid Saturation

4.1.1. Calculation of T_2 Cut-Off Value at Different Temperatures. The method mentioned above is used to calculate the T_2 cut-off value. Figure 20 shows the T_2 cut-off values at room temperature. Obviously, with the temperature being 25°C, the T_2 cut-off value is 0.092 ms. According to this method, the T_2 cut-offs at diverse temperatures are measured in Figure 21. The T_2 cut-off value increases continuously with the increase in temperature, which is mainly due to the rise in pore number and size, leading to the increase in rock permeability.

4.1.2. Variation of Movable Fluid Saturation at Different Temperatures. Figure 22 displays the correlation between the movable water saturation and temperature. According to the figure, the movable fluid saturation generally increases with increasing temperature. The growth rate is not apparent when the temperature reaches below 400°C, and the growth rate is not apparent. This is primarily due to that

the heat treatment temperature does not form large pores, and the connectivity between microcracks is not apparent, which can be found in Figure 23(a). With the temperature higher than 500°C, the increase of movable fluid saturation becomes more prominent, and the width and quantity of microcracks are larger. At 600°C, movable fluid saturation reaches 45.5%, much higher than 21.2% at 25°C. At this time, the microcracks between different bedding have been connected.

Through the analysis of experimental results, the proportion of movable fluid saturation progressively enhances, and the pore connectivity is enhanced in the pyrolysis temperature range. Elevated temperature favors the transport of pyrolysis products from oil shale.

4.2. Relationship between Movable Fluid Saturation and Porosity and Permeability Characteristics. Figure 24 presents the correction between movable fluid saturation and porosity. According to the figure, when porosity constantly increases, movable fluid saturation rises continuously. When the porosity is lower than 22.5% (heat treatment temperature is 600°C), the increase of movable fluid saturation is apparent; with the continuous improvement of porosity, the growth rate of movable fluid saturation decreases significantly.

The association of permeability with the saturation of mobile fluid is depicted in Figure 25. As is clear, the two parameters exhibit approximate linearity. The saturation of mobile fluid increases persistently as the permeability value progressively increases.

5. Conclusion

To conclude, the findings of the pyrolysis experiments and NMR and FE-SEM tests on oil shale samples from the Jimsar Sag area demonstrated the impacts of pyrolysis on shale pore structures. The T_2 relaxation spectra, pore size distribution, and pore and permeability variation were analyzed. The T_2 cut-off value and movable fluid saturation at different thermal treatment temperatures were calculated, and the relationships between movable fluid saturation and porosity and permeability were calculated and fitted separately. The conclusions are presented as follows:

(1) With the enhancing heat treatment temperature, the size and number of pores and microcracks increase. The oil shale is comparatively dense at room temperature, and irregular pores and fractures are distributed in the rock matrix. When the heat treatment temperature increases, tiny pores of thermal stress increase and gradually polymerize into medium and large pores; Microcracks continue to extend and expand and slowly realize connectivity. 500°C~600°C is an essential pore and microcrack development stage

(2) Pyrolysis increases the porosity of oil shale. With increasing thermal treatment temperature, the porosity of oil shale increase continuously. When the temperature is lower than 400°C, the porosity and permeability increase slowly, increasing by 16.85% and 16.96%, respectively, compared with room temperatures. With the thermal treatment temperature higher than 500°C, the growth rate of porosity increases rapidly

(3) The increase of pores and microcracks inevitably leads to an increase in permeability. In the pyrolysis temperature range of 25°C~400°C, the growth rate of permeability is relatively slow. With the constant temperature increase (500°C~600°C), the growth rate of permeability accelerates rapidly; when the temperature increases (700°C), the permeability increase begins to slow down

(4) With the constant increase of heat treatment temperature, the movable fluid saturation increases significantly, and the effect is the most significant when the heat treatment temperature reaches 500°C~600°C. There is a nonlinear correlation between porosity and movable fluid saturation and a linear correlation between permeability and movable fluid saturation. In addition, 600°C is the suitable temperature for the pyrolysis of oil shale

Data Availability

Data are available on corresponding author request.

Conflicts of Interest

The authors declare no conflict of interest.

Acknowledgments

This study was funded by the National Natural Science Foundation of China "Research on the evolutionary mechanism of casing deformation and control measures based on the 4-dimensional geomechanics during fracturing" (52004013).

References

[1] L. K. Huang, J. J. Liu, F. S. Zhang, E. Dontsov, and B. Damjanac, "Exploring the influence of rock inherent heterogeneity and grain size on hydraulic fracturing using discrete element modeling," *International Journal of Solids and Structures.*, vol. 176-177, pp. 207–220, 2019.

[2] H. Suyun, Z. Wenzhi, H. Lianhua et al., "Development potential and technical strategy of continental shale oil in China," *Petroleum Exploration and Development*, vol. 47, no. 4, pp. 877–887, 2020.

[3] W. Taciuk, "Editor's page. Does oil shale have a significant future?," *Oil Shale*, vol. 30, no. 1, pp. 1–5, 2013.

[4] M. Yue, T. Y. Song, Q. Chen et al., "Prediction of effective stimulated reservoir volume after hydraulic fracturing utilizing deep learning," *Petroleum Science and Technology*, pp. 1–23, 2022.

[5] Z. Wenzhi, H. Suyun, H. Lianhua et al., "Types and resource potential of continental shale oil in China and its boundary

with tight oil," *Petroleum Exploration and Development*, vol. 47, no. 1, pp. 1–11, 2020.

[6] J. G. Na, C. H. Im, S. H. Chung, and K. B. Lee, "Effect of oil shale retorting temperature on shale oil yield and properties," *Fuel*, vol. 95, pp. 131–135, 2012.

[7] P. Tan, H. W. Pang, R. X. Zhang et al., "Experimental investigation into hydraulic fracture geometry and proppant migration characteristics for southeastern Sichuan deep shale reservoirs," *Journal of Petroleum Science and Engineering*, vol. 184, article 106517, 2020.

[8] G. Zhu, B. Zhang, P. Zhao et al., "Upgrading low-quality oil shale using high-density gas-solid fluidized bed," *Fuel*, vol. 252, pp. 666–674, 2019.

[9] F. Y. Wang and L. Wang, "Pore structure analysis and permeability prediction of shale oil reservoirs with HPMI and NMR: a case study of the Permian Lucaogou Formation in the Jimsar Sag, Junggar Basin, NW China," *Journal of Petroleum Science and Engineering*, vol. 214, p. 110503, 2022.

[10] K. G. Hazra, *Comparison of Heating Methods for In-Situ Oil Shale Extraction*, Texas A & M University, 2014, (PhD thesis).

[11] K. J. Lee, *Rigorous Simulation Model of Kerogen Pyrolysis for the In-Situ Upgrading of Oil Shales*, Texas A &M University, 2014, (PhD thesis).

[12] L. Wang, Y. Zhao, D. Yang, Z. Kang, and J. Zhao, "Effect of pyrolysis on oil shale using superheated steam: a case study on the Fushun oil shale, China," *Fuel*, vol. 253, pp. 1490–1498, 2019.

[13] S. Wang, X. Jiang, X. Han, and J. Tong, "Investigation of Chinese oil shale resources comprehensive utilization performance," *Energy*, vol. 42, no. 1, pp. 224–232, 2012.

[14] L. W. Pan, F. Q. Dai, S. H. Pei, J. Huang, and S. Liu, "Influence of particle size and temperature on the yield and composition of products from the pyrolysis of Jimsar (China) oil shale," *Journal of Analytical and Applied Pyrolysis*, vol. 157, article 105211, 2021.

[15] Y. M. Zhai, Y. M. Zhu, S. Cui, Y. Tao, X. Kai, and T. Yang, "Study on the co-pyrolysis of oil shale and corn stalk: pyrolysis characteristics, kinetic and gaseous product analysis," *Journal of Analytical and Applied Pyrolysis*, vol. 163, article 105456, 2022.

[16] H. L. Zhan, F. K. Qin, S. T. Chen et al., "Two-step pyrolysis degradation mechanism of oil shale through comprehensive analysis of pyrolysis semi-cokes and pyrolytic gases," *Energy*, vol. 241, article 122871, 2022.

[17] Z. Kang, D. Yang, Y. Zhao, and Y. Hu, "Thermal cracking and corresponding permeability of Fushun oil shale," *Oil shale*, vol. 28, no. 2, pp. 273–283, 2011.

[18] T. Saif, Q. Y. Lin, B. Bijeljic, and M. J. Blunt, "Microstructural imaging and characterization of oil shale before and after pyrolysis," *Fuel*, vol. 197, pp. 562–574, 2017.

[19] P. Tiwari, M. Deo, C. L. Lin, and J. D. Miller, "Characterization of oil shale pore structure before and after pyrolysis by using X-ray micro CT," *Fuel*, vol. 107, pp. 547–554, 2013.

[20] C. Ma, X. Z. Zhao, T. Yang et al., "Mineralogy, organic geochemistry, and microstructural characterization of lacustrine Shahejie Formation, Qikou Sag, Bohai Bay Basin: contribution to understanding microcosmic storage mechanism of shale oil," *Journal of Petroleum Science and Engineering*, vol. 209, article 109843, 2022.

[21] W. Song, J. Yao, K. Zhang, Y. Yang, and H. Sun, "Understanding gas transport mechanisms in shale gas reservoir: pore network modelling approach," *Advances in Geo-Energy Research*, vol. 6, no. 4, pp. 359-360, 2022.

[22] W. R. Wang, D. L. Yue, K. A. Eriksson et al., "Qualitative and quantitative characterization of multiple factors that influence movable fluid saturation in lacustrine deep-water gravity-flow tight sandstones from the Yanchang Formation, southern Ordos Basin, China," *Marine and Petroleum Geology*, vol. 121, article 104625, 2020.

[23] C. F. Zhu, W. Guo, Y. J. Li, H. Gong, J. J. Sheng, and M. Dong, "Effect of occurrence states of fluid and pore structures on shale oil movability," *Fuel*, vol. 288, article 119847, 2021.

[24] C. Liu, L. Zhang, Y. Li, F. Liu, D. A. Martyushev, and Y. Yang, "Effects of microfractures on permeability in carbonate rocks based on digital core technology," *Advances in Geo-Energy Research*, vol. 6, no. 1, pp. 86–90, 2022.

[25] L. U. Shuangfang, X. U. Haitao, W. A. Min et al., "Several key issues and research trends in evaluation of shale oil," *Acta Petrolei Sinica*, vol. 37, no. 10, pp. 1309–1322, 2016.

[26] Q. Sang, S. Zhang, Y. Li, M. Dong, and S. Bryant, "Determination of organic and inorganic hydrocarbon saturations and effective porosities in shale using vacuum-imbibition method," *International Journal of Coal Geology*, vol. 200, pp. 123–134, 2018.

[27] Y. D. Cai, D. M. Liu, Z. J. Pan, Y. Yao, J. Li, and Y. Qiu, "Petrophysical characterization of Chinese coal cores with heat treatment by nuclear magnetic resonance," *Fuel*, vol. 108, pp. 292–302, 2013.

[28] C. Lyu, Z. Ning, Q. Wang, and M. Chen, "Application of NMR T2 to pore size distribution and movable fluid distribution in tight sandstones," *Energy & Fuels*, vol. 32, no. 2, pp. 1395–1405, 2018.

[29] X. J. Wang, Y. Song, X. G. Guo et al., "Pore-throat structure characteristics of tight reservoirs of the Middle Permian Lucaogou formation in the Jimsar Sag, Junggar Basin, northwest China," *Journal of Petroleum Science and Engineering*, vol. 208, article 109245, 2022.

[30] L. Yang, N. H. Dou, X. B. Lu et al., "Advances in understanding imbibition characteristics of shale using an NMR technique: a comparative study of marine and continental shale," *Journal of Geophysics and Engineering*, vol. 15, no. 4, pp. 1363–1375, 2018.

[31] R. X. Zhao, H. T. Xue, S. F. Lu et al., "Multi-scale pore structure characterization of lacustrine shale and its coupling relationship with material composition: an integrated study of multiple experiments," *Marine and Petroleum Geology*, vol. 140, article 105648, 2022.